The Astrophysical Journal, 940:93 (13pp), 2022 November 20 https://doi.org/10.3847/1538-4357/ac8f44

On the Characterization of GJ 504: A Magnetically Active Planet-host Star Observed by the Transiting Exoplanet Survey Satellite (TESS)

Maria Pia Di Mauro[1], Raffaele Reda[1,2], Savita Mathur[3,4], Rafael A. García[5], Derek L. Buzasi[6], Enrico Corsaro[7], Othman Benomar[8,9], Lucía González Cuesta[3,4], Keivan G. Stassun[10,11], Serena Benatti[12], Valentina D'Orazi[13,14], Luca Giovannelli[1,2], Dino Mesa[13], and Nicolas Nardetto[15]
[1] INAF-IAPS, Istituto di Astrofisica e Planetologia Spaziali, Via del Fosso del Cavaliere 100 I-00133 Roma, Italy; maria.dimauro@inaf.it
[2] Dipartimento di Fisica, Università di Roma Tor Vergata, Via della Ricerca Scientifica 1, I-00133 Roma, Italy
[3] Instituto de Astrofísica de Canarias (IAC), E-38205 La Laguna, Tenerife, Spain
[4] Universidad de La Laguna (ULL), Departamento de Astrofísica, E-38206 La Laguna, Tenerife, Spain
[5] AIM, CEA, CNRS, Université Paris-Saclay, Université de Paris, Sorbonne Paris Cité, F-91191 Gif-sur-Yvette, France
[6] Dept. of Chemistry & Physics, Florida Gulf Coast University, 10501 FGCU Blvd. S., Fort Myers, FL 33965 USA
[7] INAF-Astrophysical Observatory of Catania, Via S. Sofia 78 I-95123 Catania, Italy
[8] National Astronomical Observatory of Japan, Mitaka, Tokyo, Japan
[9] Center for Space Science, New York University Abu Dhabi, UAE
[10] Vanderbilt University, Department of Physics & Astronomy, 6301 Stevenson Center Ln., Nashville, TN 37235, USA
[11] Vanderbilt Initiative in Data-intensive Astrophysics (VIDA), 6301 Stevenson Center Lane, Nashville, TN 37235, USA
[12] INAF—Osservatorio Astronomico di Palermo, Piazza del Parlamento 1, I-90134 Palermo, Italy
[13] INAF Osservatorio Astronomico di Padova, vicolo dell'Osservatorio 5 I-35122, Padova Italy
[14] School of Physics and Astronomy, Monash University, Clayton, VIC 3800, Australia
[15] Université Côte d'Azur, Observatoire de la Côte d'Azur, CNRS, Laboratoire Lagrange, France
Received 2022 February 25; revised 2022 September 1; accepted 2022 September 2; published 2022 November 23

Abstract

We present the results of the analysis of the photometric data collected in long- and short-cadence mode by the Transiting Exoplanet Survey Satellite for GJ 504, a well-studied planet-hosting solar-like star, whose fundamental parameters have been largely debated during the last decade. Several attempts have been made by the present authors to isolate the oscillatory properties expected on this main-sequence star, but we did not find any presence of solar-like pulsations. The suppression of the amplitude of the acoustic modes can be explained by the high level of magnetic activity revealed for this target, not only by the study of the photometric light curve but also by the analysis of three decades of available Mount Wilson spectroscopic data. In particular, our measurements of the stellar rotational period $P_{\rm rot} \simeq 3.4$ days and of the main principal magnetic cycle of $\simeq$12 yr confirm previous findings and allow us to locate this star in the early main-sequence phase of its evolution during which the chromospheric activity is dominated by the superposition of several cycles before the transition to the phase of the magnetic-braking shutdown with the subsequent decrease of the magnetic activity.

Unified Astronomy Thesaurus concepts: Asteroseismology (73); Stellar rotation (1629); Magnetic variable stars (996); A stars (5); Exoplanet systems (484); Stellar oscillations (1617); Stellar properties (1624)

1. Introduction

Over the last decade, thanks to the successful photometric space missions Convection, Rotation, and Transits (CoRoT; Baglin et al. 2006) and Kepler/K2 (Borucki et al. 2010), mainly conceived for exoplanets, but extremely suitable for detection of stellar pulsations, asteroseismology has produced an extraordinary revolution in astrophysics (e.g., Beck et al. 2012; Bedding et al. 2011; Silva Aguirre et al. 2015; Stello et al. 2016). This unveiled a wealth of results on the physical properties of stars over a large part of the Hertzprung-Russell (H-R) diagram and mostly for solar-like stars, which exhibit pulsations excited by near-surface turbulent convection, as it happens in the Sun.

The extreme photometric precision made these missions spectacularly successful also in their primary goal: the detection and characterization of extrasolar planetary systems by using the transit technique (Borucki et al. 2013). Thus, in recent years, a flood of very high-quality data has been collected, and the search for new worlds is in progress, and we are living exciting times in this respect. Despite the incredible effort in refining observational and post-processing techniques, our interpretation and comprehension of planetary systems architecture, formation, and evolution mechanisms heavily relies on the accuracy of the inferred characteristics of the host stars and the effects on their planets (Van Eylen et al. 2014; Borucki et al. 2013; Huber et al. 2013; Chaplin et al. 2013). This often represents a significant challenge, especially for isolated field stars (Soderblom et al. 2014).

The most recently launched NASA space mission Transiting Exoplanet Survey Satellite (TESS; Ricker et al. 2014) is poised to continue the synergy between asteroseismology and exoplanet science, enlarging the held asteroseismic inference to full-sky. Indeed, with the original high-cadence mode of 120 s (Nyquist frequency of 4166 μHz) used during the first 2 yr of its main mission and the newer fast cadence of 20 s that started during the extended mission, TESS should be able to detect oscillations in many main-sequence solar-like stars in spite of their low intrinsic amplitudes of parts per million (ppm; García & Ballot 2019).

According to the TESS Asteroseismic Target List (Campante et al. 2016; Schofield et al. 2019), thousands of main-sequence and subgiant solar-like stars should show detectable modes. So

far, signatures of such oscillations have been detected only in a handful of solar-like stars (e.g., Gandolfi et al. 2018; Huber et al. 2019; Chontos et al. 2021; Metcalfe et al. 2020; Addison et al. 2021; Metcalfe et al. 2021). Recently, Huber et al. (2022) compared the power spectra of three stars observed by TESS with both cadences of 120 s and 20 s. While the modes were barely visible with the 2 minutes cadence, the faster cadence drastically increased by ∼30% the signal-to-noise ratio allowing the characterization of the individual modes. Part of this improvement could be explained by the difference of the cosmic-ray rejection applied to both cadences. However, the difficulties to detect the oscillation modes could also be due to the properties of the stars.

The nondetection of modes has been investigated also in many stars observed by the Kepler mission. For solar-like stars, the usual explanation is the surface magnetic activity of the star (e.g., Chaplin et al. 2011a) as it is known that a high level of magnetic activity can reduce the amplitude of the modes (García et al. 2010; Kiefer et al. 2017; Santos et al. 2018). Nevertheless this is not the only culprit as shown in Mathur et al. (2019). Indeed metallicity or binarity can also have an impact on the amplitude of the modes (Gaulme et al. 2020). For the binarity explanation, Gaulme et al. (2020) and Benbakoura et al. (2021) showed that synchronized binaries can have enhanced magnetic activity, which subsequently leads to suppressed modes. So in that case, magnetic activity is again the origin of the nondetection.

Here, we present the result of the analysis of the solar-type star GJ 504 (spectral type G0), which was observed by the TESS mission for 27 days during sector 23 from 2020 March 18 to 2020 April 16 using 120 s cadence mode and again during sector 50 for 27 days from 2022 March 26 to 2022 April 22, using 20 s cadence mode. Furthermore, spectroscopic observations from the Mount Wilson Observatory (MWO) are also studied to better characterize the surface magnetic activity of the star.

GJ 504 is considered a very interesting case study, claimed to host a substellar companion whose nature is strongly debated. Nevertheless, asteroseismology might provide the only powerful mean to dissolve any doubts about the evolutionary state of this target and hence on the identity of the secondary object. In fact, the detection of typical signatures of solar-like oscillations in the power spectrum would define with good accuracy the age and all the physical parameters of this low-mass star (e.g., Di Mauro et al. 2004; Di Mauro 2017). There are many methods to estimate the age of a single star (Soderblom et al. 2014): empirical indicators such as stellar activity and gyrochronology, which link rotation to age (e.g., Skumanich 1972; Barnes 2007; Mamajek & Hillenbrand 2008); photospheric lithium abundance (e.g., Li et al. 2012); comparison of stellar model isochrones with observed classical parameters (e.g., Pont & Eyer 2004). However, the accuracy that can currently be reached by using all these methods is not satisfactory, not only because of the large errors in the estimates but also because better precision and accuracy can be reached only by using seismic diagnostics (see, e.g., Metcalfe et al. 2010; Lebreton et al. 2014; Lebreton & Goupil 2014).

This paper is organized in the following sections: Section 2 introduces the reader to the target presenting the spectroscopic fundamental parameters and the theoretical predictions deduced by means of stellar evolutionary models and asteroseismic scaling laws; Section 3 presents the observations and the data calibration used in this work; in Section 4, we study the surface rotation and magnetic activity of the star; in Section 5, we describe the search for solar-like oscillations; Section 6 discusses the reasons for the nondetection of solar-like oscillations; Section 7 shows the conclusions on our attempt to characterize the structure of this star.

2. The Solar-like Star GJ 504

2.1. An Intriguing Case

During the last 25 yr, several dedicated space missions, together with great developments in observational techniques, have allowed huge progresses in the search for new worlds outside the solar system. In particular, besides statistics, several hundreds of bright stars have been monitored and multi-wavelengths data collected to understand and characterize the formation and the evolution of the already-discovered planetary systems.

A controversial case still debated today is represented by the solar-type star GJ 504 (HD 115383, TIC 397587084), a G0-type star with $T_{\rm eff} \approx 6200\,K$, which appears to be a little more massive than the Sun (Kuzuhara et al. 2013; D'Orazi et al. 2017), with a rotational period $P_{\rm rot} = 3.329$ days, average of the values reported by Messina et al. (2003) and Donahue et al. (1996). In 2013, by exploiting high-contrast near-IR and L' band observations as part of the SEEDS survey, Kuzuhara et al. (2013) reported the direct-imaging discovery of a Jovian planet orbiting this star, with a projected separation of 43.5 au. Unfortunately, no radial velocity data are available for the host star, and hence the mass of the planet needs to be estimated in other ways. Employing the gyrochronology technique, based on the stellar chromospheric activity indices (as given by the Ca II H and K emission lines) and on X-ray observations (the star is included in the ROSAT catalog), Kuzuhara et al. (2013) estimated the age of GJ 504 to be Age $= 160^{+350}_{-60}$ Myr. Under this age assumption, the comparison of the observed planet's luminosity at each band with the theoretical models by Baraffe et al. (2003) implies that the mass of the substellar companion (named GJ 504b) should be $M_{\rm P} = 4^{+4.5}_{-1.0}\,M_{\rm Jup}$. According to Kuzuhara et al. (2013), the measured characteristics make GJ 504b a very interesting object because it represents the first example of giant planet on a wide orbit around a solar-type star. Moreover, the planet appears to be significantly cool ($T_{\rm eq} = 510^{+30}_{-20}$ K), with an almost-cloud-free atmosphere due to its blue color (J–H $= -0.23$), and as reported by Janson et al. (2013), it represents the first known extrasolar planet with methane-dominated atmosphere (T-type).

However, a few years later, the young age of GJ 504 has been disproved by Fuhrmann & Chini (2015), thanks to evidences arising from high-resolution and high-quality spectra. In fact, the authors derived a stellar gravity of $\log g = 4.23$ dex (from the Hipparcos parallax and adopting spectroscopic temperature), which results to be not compatible with a stellar age of few hundreds Myr. This gravity estimate is also in agreement with the value of $\log g = 4.17$ dex previously determined in Fuhrmann (2004), based on the spectral fitting of Mg Ib lines and several independent spectroscopic studies and position of the star in the color–magnitude diagram (see, e.g., da Silva et al. 2012). This picture implies that GJ 504 should be a star with approximately the solar age, and as a consequence, the companion has to be identified as a brown dwarf

($M_P \sim 25 M_{Jup}$) rather than a giant planet. To explain the relatively high stellar rotation velocity and chromospheric activity level of the host star, and reconcile the isochronal ages with direct indicators, Fuhrmann & Chini (2015) invoked a merging event. GJ 504 might have engulfed a substellar companion that is responsible for speeding up the rotational velocity and accounts for the enhanced activity levels (Oetjens et al. 2020).

D'Orazi et al. (2017), reassessing the properties of GJ 504, have found that the surface gravity of the star implies an evolutionary stage obtained by the isochrones comparison, which suggests an age range between 1.8 and 3.5 Gyr (most probable age ≈2.5 Gyr). To reconcile all the age indicators and to explain the high level of activity, also these authors suggest a merging scenario (more recent than 200 Myr) with a very close hot Jupiter companion.

The system has been recently revisited by Bonnefoy et al. (2018) by using interferometric, radial-velocity, and high-contrast imaging observations. They found an interferometric radius of $R = (1.35 \pm 0.04) R_\odot$ for GJ 504, which is compatible with two isochronal age ranges (21 ± 2) Myr and (4.0 ± 1.8) Gyr. According to this work, the mass of GJ 504b is expected to be $M_P = 1.3^{+0.6}_{-0.3}\ M_{Jup}$ for the young-age case and $M_P = 23^{+10}_{-9}\ M_{Jup}$ for the old one.

Therefore, the evolutionary stage and the age of GJ 504 are still an open problem with no clear solution to date. This uncertainty closely concerns the mass estimation of the star's companion, which could be a Jovian planet or a brown dwarf. In addition, Skemer et al. (2016), through a photometric study, suggested for GJ 504b a higher metallicity ($[M/H]_p \approx +0.6$) with respect to the host star ($[M/H]_\star \approx +0.1$–0.3), adding to this system another element of interest.

For all the above mentioned reasons, the GJ 504 system constitutes an intriguing case, which deserves to be carefully studied, with the aim of shedding light on the age of the star and, accordingly, on the nature of the substellar companion.

2.2. Fundamental Parameters

With the aim to properly characterize this star, we performed an analysis of the broadband spectral energy distribution (SED) together with the Gaia EDR3 (Gaia Collaboration 2018) parallax measurement following the procedures described in Stassun & Torres (2016); Stassun et al. (2017), and Stassun et al. (2018). The input parameters and the obtained results are summarized in Table 1. We employed the *UBV* magnitudes from Mermilliod (2006), the $B_T V_T$ magnitudes from *Tycho-2*, the Strömgren *uvby* magnitudes from Paunzen (2015), the JHK_S magnitudes from Two Micron All Sky Survey, the W1–W4 magnitudes from Wide-field Infrared Survey Explorer (WISE), and the far-UV magnitude from Galaxy Evolution Explorer (GALEX). The available photometry, all together, spans the full stellar SED over the wavelength range 0.2–22 μm (Figure 1).

We performed a fit using Kurucz stellar atmosphere models, with the $T_{\rm eff}$, $\log g$, [Fe/H], and $v \sin i$ taken from the spectroscopic analysis of D'Orazi et al. (2017). The remaining parameter is the extinction (A_V), which we fixed to be zero due to the star's proximity. The resulting fit is shown in Figure 1, obtained with a reduced $\chi^2 = 1.9$. Integrating the SED fitting model, we obtain the bolometric flux at Earth of $F_{\rm bol} = (2.096 \pm 0.024) \cdot 10^{-7}$ erg s^{-1} cm^{-2}. Taking the $F_{\rm bol}$ and $T_{\rm eff}$ together with the Gaia parallax, with no adjustment for systematic parallax offset (see, e.g., Stassun & Torres 2021), gives

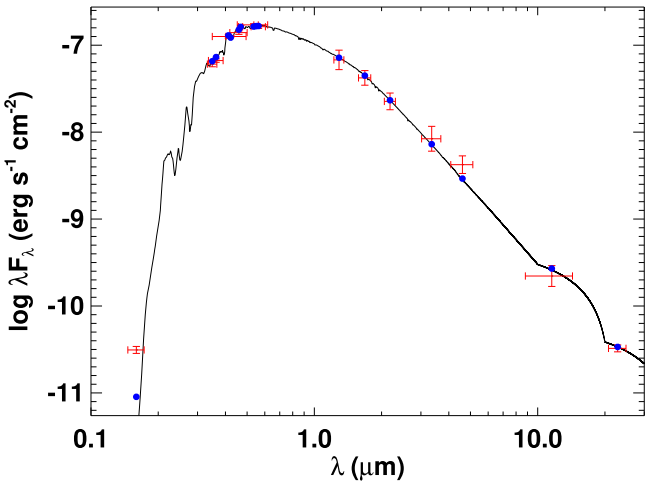

Figure 1. Spectral energy distribution. Red symbols represent the observed photometric measurements, where the horizontal bars represent the effective width of the passband. Blue symbols are the model fluxes from the best-fit Kurucz atmosphere model (black).

Table 1
The Fundamental Parameters of GJ 504 (TIC 397587084)

Basic Properties	
TESS Magnitude	4.6552 ± 0.0073[a]
π (mas)	57.0186 ± 0.2524[b]
Spectroscopic Parameters[c]	
$T_{\rm eff}$ (K)	6205 ± 20
[Fe/H] (dex)	0.22 ± 0.04
$v \sin i$ (km s^{-1})	2.8 ± 1.6
$\log g$ (dex)	4.29 ± 0.07
SED Results	
$F_{\rm bol}$ (erg s^{-1} cm^{-2})	$(2.10 \pm 0.02) \cdot 10^{-8}$
$L_{\rm SED}/L_\odot$	2.01 ± 0.03
$M_{\rm SED}/M_\odot$	1.07 ± 0.17
$R_{\rm SED}/R_\odot$	1.227 ± 0.012
$P_{\rm SED}$(d)	2.4 ± 1.3
$Age_{\rm SED}$(Gyr)	0.2 ± 0.2
SBCR Results	
$\theta_L D$ (mas)	0.622 ± 0.122
$R_{\rm SBCR}/R_\odot$	1.176 ± 0.192

Notes.
[a] Adopted from the TESS Input Catalog (Stassun et al. 2019).
[b] Gaia measurement (see Gaia Collaboration 2018).
[c] Determined by spectroscopic observations (see D'Orazi et al. 2017).

the stellar radius as $R_{\rm SED} = (1.227 \pm 0.012) R_\odot$. The $F_{\rm bol}$ and parallax also yield directly the bolometric luminosity, $L_{\rm SED} = (2.01 \pm 0.03) L_\odot$.

The empirical stellar radius determined above affords an opportunity to estimate the stellar mass empirically as well, via the spectroscopically determined surface gravity, obtaining $M_{\rm SED} = (1.07 \pm 0.17)\, M_\odot$. This value is consistent with that estimated via the eclipsing-binary-based relations of Torres et al. (2010).

Using the activity–age relations of Mamajek & Hillenbrand (2008), we obtained, from $R'_{\rm HK}$ and the star's $B - V$ color, an

age of (0.2 ± 0.2) Gyr and a rotational period for the star of $P_{\rm SED} = (2.4 \pm 1.3)$ days, which is consistent with previous findings of 3.3 days (Donahue et al. 1996; Messina et al. 2003; Wright et al. 2011).

To get another independent measurement of the stellar radius, it is also possible to employ the approach based on the surface-brightness–color relationships (SBCR), which allows to easily estimate the limb-darkened angular diameter of the star. The latter combined with the distance of the star provides the linear stellar radius.

Considering the SBCR from Salsi et al. (2021) obtained for late-type dwarf stars (their Table 4), $m_G = 5.0398 \pm 0.0029$ mag (Gaia Collaboration 2020), $m_{K_s} = 4.033 \pm 0.238$ mag (Cutri et al. 2003), and the extinctions in the visual and Gaia bands $A_v = A_g = 0.0$ mag derived from `Stilism` tool (Lallement et al. 2014; Capitanio et al. 2017), as well as $A_k = 0.089 A_v$ (Nishiyama et al. 2009); we find $\theta_{LD} = 0.622 \pm 0.014 \pm 0.008 \pm 0.100$ mas. The uncertainties correspond respectively to the rms of the SBCR, the uncertainty on the coefficients of the SBCR, and the uncertainty on the G and Ks photometries. Using Gaia DR2 parallax, i.e., $\pi = 56.8577 \pm 0.1224$ mas (Gaia Collaboration 2020), we obtain $R_{SBCR} = (1.176 \pm 0.027 \pm 0.015 \pm 0.19 \pm 0.003)\,R_\odot = (1.176 \pm 0.192) R_\odot$, where the error 0.003 is rising from the uncertainty on the Gaia parallax. This value agrees within the uncertainty with the SED estimate found above.

2.3. The Seismic Properties and the Asteroseismic Prediction by Scaling Laws

The properties of a solar-like pulsating star can be described by adopting the asymptotic development by Tassoul (1980), which predicts that the oscillations excited in main-sequence stars are acoustic modes (p modes) with frequencies $\nu_{n,l}$ characterized by radial order n and harmonic degree l, which for $l \leqslant n$ should satisfy the following approximation:

$$\nu_{n,l} \sim \Delta\nu \left(n + \frac{l}{2} + \epsilon \right), \tag{1}$$

where ϵ is a function of frequency and depends on the properties of the surface layers, and $\Delta\nu$, known as the large frequency separation, is the inverse of the sound travel time across the stellar diameter

$$\Delta\nu = \left(2 \int_0^R \frac{\mathrm{d}r}{c} \right)^{-1}, \tag{2}$$

where c is the local speed of sound at radius r, and R is the photospheric stellar radius. Hence, according to the theory, the solar-like oscillations spectrum of GJ 504 should show a series of equally spaced peaks separated by $\Delta\nu$ between p modes of same degree l and adjacent n:

$$\Delta\nu \simeq \nu_{n+1,l} - \nu_{n,l} \equiv \Delta\nu_l. \tag{3}$$

In addition, the power spectra of this target should show another series of peaks, whose separation $\delta\nu_l$ is known as the small separation:

$$\delta\nu_l \equiv \nu_{n,l} - \nu_{n-1,l+2}, \tag{4}$$

which is sensitive to the chemical composition gradient in the central regions of the star and hence to its evolutionary state. Thus, the determination of the large and small frequency separations from the observed oscillation spectrum can directly provide asteroseismic inferences on the mass and the age of GJ 504 (Christensen-Dalsgaard 1988).

Table 2
Predictions for the Frequency of Maximum Oscillation Computed Assuming Spectroscopic Data Obtained by Different Authors

$T_{\rm eff}$ (K)	log g (dex)	$\nu_{\rm max}$ (μHz)	Reference
6205 ± 20	4.29 ± 0.07	2096 ± 338	D'Orazi et al. (2017)
5978 ± 60	4.23 ± 0.10	1860 ± 428	Fuhrmann & Chini (2015)
6130 ± 48	4.33 ± 0.10	2312 ± 533	Maldonado et al. (2015)
6185 ± 51	4.30 ± 0.07	2148 ± 346	Battistini & Bensby (2015)
5995 ± 41	4.24 ± 0.02	1900 ± 88	Ramírez et al. (2013)
6012 ± 100	4.30 ± 0.20	2179 ± 100	Mishenina et al. (2013)
6234 ± 25	4.60 ± 0.02	4269 ± 197	Valenti & Fischer (2005)

The observed oscillation power spectrum of the solar-like stars is characterized by a typical Gaussian-like envelope, and the frequency of maximum oscillation power is usually indicated by $\nu_{\rm max}$. As conjectered by Brown et al. (1991), the frequency $\nu_{\rm max}$ can be related to the acoustic cutoff frequency $\nu_{\rm ac}$, which defines the upper boundary of the p mode resonant cavities:

$$\nu_{\rm max} \propto \nu_{\rm ac} \propto g T_{\rm eff}^{-1/2}. \tag{5}$$

Thus, according to Equation (5), the frequency $\nu_{\rm max}$ carries information on the physical conditions in the near-surface layers of the star. Thus, as it has been well demonstrated both theoretically (Chaplin et al. 2008; Belkacem et al. 2011) and observationally (Bedding & Kjeldsen 2003; Stello et al. 2008; Bedding 2014), as a solar-type star evolves, its oscillation spectrum moves toward lower frequencies due to the decrease of the surface gravity.

To extract a rough estimate of the asteroseismic parameters of the star to be adopted as guess values for the oscillation analysis, it is possible to assume well-proved scaling laws as those provided by Brown et al. (1991), Kjeldsen & Bedding (1995), and Huber et al. (2011). These relations, which have been typically calibrated on large samples of main-sequence stars, offer the possibility to predict the range of frequencies where the excess of power for a given solar-like star will manifest. By assuming the relations by Kjeldsen & Bedding (1995) and Kjeldsen et al. (2008), we calculated the value of the expected maximum amplitude of oscillation $A_{\rm max}$ and the frequency at the maximum amplitude $\nu_{\rm max}$, using the observed surface gravity g and the effective temperature $T_{\rm eff}$ of the star. By using scaling relations and corrections by Campante et al. (2016), we obtained a value for the expected maximum amplitude in the range $A_{\rm max} = (2.51\text{–}2.95)$ parts per million depending on which input spectroscopic parameters are assumed.

Table 2 shows the results for the expected $\nu_{\rm max}$ computed assuming spectroscopic measurements published by different authors. Except for the $\nu_{\rm max}$ from the stellar parameters of Valenti & Fischer (2005), who reported a high surface gravity, all the expected values for the frequency of maximum oscillation lie in the range (1800–2300) μHz. Thus, if there is an excess of power due to oscillations in the GJ 504 spectrum, we expect to find it in this range of frequencies.

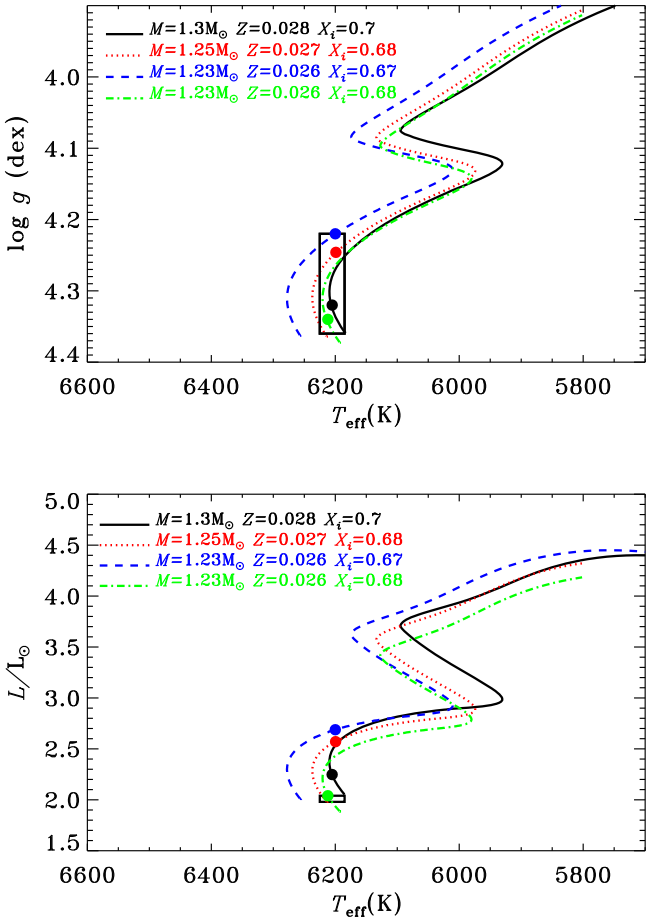

Figure 2. Evolutionary tracks plotted in two plans of the H-R diagram calculated for different values of the mass and the metallicity, while all the other parameters are fixed. The initial hydrogen abundance is X_i, and the mixing-length coefficient is $\alpha = 1.8$. The rectangle defines the 1σ error box for the observed gravity and effective temperature. Colored dots indicate the position of the four structure models (see Table 3), which best reproduce the observations of GJ 504.

2.4. Theoretical Prediction by Evolutionary Models

Given the observed fundamental parameters collected in Table 1, it is also possible to face the theoretical challenge to infer the structural properties of GJ 504 and predict its detailed oscillation spectrum by constructing stellar evolutionary models that satisfy the observational constraints.

We produced theoretical structure models for the star by using the ASTEC evolutionary code (Christensen-Dalsgaard 2008a) by varying the mass and the composition so to match the atmospheric parameters available. The resulting evolutionary tracks characterized by the fixed mass M and initial chemical composition have been calculated with the OPAL 2005 equation of state (Rogers & Nayfonov 2002), OPAL opacities (Iglesias & Rogers 1996), and the NACRE nuclear reaction rates (Angulo et al. 1999). Convection was treated according to the mixing-length formalism (MLT; Böhm-Vitense 1958) and defined through the parameter $\alpha = \ell/H_p$, where H_p is the pressure scale height, and α is assumed to be 1.8. The initial heavy-element mass fraction Z in respect to the abundance of the hydrogen X has been calculated from the iron abundance given in Table 1 using the relation $[\mathrm{Fe/H}] = \log(Z/X)_s - \log(Z/X)_\odot$, where $(Z/X)_s$ is the value at the stellar surface, and the solar value was taken to be $(Z/X)_\odot = 0.0245$ (Grevesse & Noels 1993).

Table 3
Main Parameters for Four Best-fit Structure Models of GJ 504

	Model 1	Model 2	Model 3	Model 4
$M/\mathrm{M}_\odot$	1.23	1.23	1.25	1.30
Age (Gyr)	0.66	2.46	2.19	0.74
$T_{\rm eff}$ (K)	6212	6200	6200	6205
$\log g$ (dex)	4.34	4.22	4.25	4.32
$R/\mathrm{R}_\odot$	1.23	1.42	1.38	1.30
$L/\mathrm{L}_\odot$	2.04	2.69	2.57	2.25
Z_s	0.026	0.026	0.027	0.028
X_s	0.68	0.67	0.68	0.7
X_c	0.58	0.29	0.35	0.59
[Fe/H]	0.19	0.20	0.21	0.21
r_{cz}/R	0.840	0.837	0.846	0.846
α_{MLT}	1.8	1.8	1.8	1.8
$\Delta\nu$ (μHz)	109.6	87.8	90.9	104.5

Note. $M/\mathrm{M}_\odot$ is the mass of the star, $T_{\rm eff}$ is the effective temperature, $\log g$ is the surface gravity, $R/\mathrm{R}_\odot$ is the surface radius, $L/\mathrm{L}_\odot$ is the luminosity, Z_s is the surface heavy-element abundance, X_s is the surface hydrogen abundance, X_c is the hydrogen abundance in the core, [Fe/H] is the iron abundance, r_{cz} is the location of the base of the convective region, α_{MLT} is the mixing-length parameter, and $\Delta\nu$ is the large separation obtained from the theoretical pulsational frequencies.

Figure 2 shows a series of evolutionary tracks obtained for different masses and a fixed initial composition, plotted in two H-R diagrams, representing respectively the effective temperature–gravity plane and the effective temperature–luminosity plane. The present evolutionary models do not include additional effects such as overshooting, settling of heavy elements, and rotation.

The location of the star in the H-R diagram identifies GJ 504 as being at the beginning of the main-sequence phase. In fact, only a small percentage of the hydrogen fuel, indicated by X_c in Table 3, has been already converted into helium. The uncertainty in the observed value of Z_s introduces an uncertainty in the determination of the stellar mass whose value, considering only the observed spectroscopic parameters, seems to be limited to the range $M = (1.28 \pm 0.07)\mathrm{M}_\odot$ hence more massive than the Sun, in agreement with the value predicted by SED analysis (see Section 2.2). The stellar radius appears $R = (1.38 \pm 0.20)\mathrm{R}_\odot$, a value that is in good agreement within the errors, not only with the estimates found in Section 2.2 by the SED and the SBCR methods but also with the most accurate interferometric radius measured by Bonnefoy et al. (2018).

The age of this star, as obtained from the evolutionary models, can be estimated in the range 0.0–2.6 Gyr, hence younger than the Sun, so that the convective envelope should appear still quite shallow with a depth not larger than $D_{cz} \simeq 0.16R$. Thus, we confirm that GJ 504 is a very young star as we found in Section 2.2 by SED calculations and in agreement, within the quoted uncertainties, with the values by D'Orazi et al. (2017) and by Kuzuhara et al. (2013), while our stellar structure models do not show a star of solar age as supposed by Fuhrmann & Chini (2015) and Bonnefoy et al. (2018).

Trying to predict the observed pulsational scenario of GJ 504, we used the ADIPLS package (Christensen-Dalsgaard 2008b) to compute theoretical adiabatic oscillation frequencies for all the structure models satisfying the spectroscopic constraints. The theoretical result shows that the oscillation modes expected to be visible in this star should be $l = 0$, 1, 2, 3 pure

acoustic modes with frequencies in the range approximately between (1500 and 3500) μHz while the theoretical large separation calculated by the linear fit over the asymptotic relation for the radial mode frequencies appears to be $\Delta\nu = (98 \pm 13)$ μHz.

Among all the possible computed structure models, we selected four models chosen to best fit the observed effective temperature, the metallicity, and the gravity (Table 1) and with location in the HR diagram shown by colored dots (see Figure 2).

In Table 3, we give a comprehensive set of physical properties for the four different models of GJ 504. In particular Model 1 has been chosen to match within 1σ the luminosity obtained by the SED technique (see Table 1).

We expect to be able to distinguish among the different models of this target by measuring at least the large separation in the observed oscillation spectrum.

3. Observations and Data Preparation

GJ 504 was observed by TESS during 27 consecutive days of sector 23 from 2020 March 18 to 2020 April 16 with a 120 s cadence mode. During the referee process of this paper, TESS Sector 50 observations from 2022 March 26 to 2022 April 22, were available including 20 s cadence data for this star. As explained later in the paper, we also analyzed these data, but the conclusions of the article remain the same. Thus, we describe all the analysis done for sector 23 with 120 s cadence data, and we only comment the new sector 50 results when relevant.

In order to perform the seismic analysis and due to the high level of noise of the TESS data for this star, we adopted four different strategies to obtain seismically optimized light curves. In such a way, we ensure that the obtained results are independent of the methodology applied.

The first methodology exploits TESS Science Processing Operations Center (SPOC; Jenkins et al. 2016) pipeline light curve, with a cadence of 120 s, available on the MAST archive.[16] This raw light curve shows strong modulations at low frequency that are filtered out by applying a smoothing removal process iterated three times. The resultant residuals are subsequently 3σ clipped to eliminate any outliers as depicted in panel (a) of Figure 3.

The second methodology started with the TESS SPOC 120 s cadence targets pixel files. We then extracted a time series for each pixel, rejecting cadences with nonzero quality flags (see for details the TESS Science Data Products Document[17]), and constructed an aperture mask using the procedure described in Buzasi et al. (2016) and Nielsen et al. (2020). Essentially this process produces a time series with the minimum sum of first differences between successive points. We then adopted σ clipping at the 4σ level combined with simple gap filling through the use of a piecewise cubic hermite interpolating polynomial (as implemented in `Scipy`; Jones et al. 2001). The result is shown in panel (b) of Figure 3.

The third approach is based on a filtering of the SPOC light curve using two successive Gaussian filters of width 0.25 and 0.125 days. These are 1D convolutional filters, as defined by the Python function `scipy.ndimage.Gaussian_filter()` (Jones et al. 2001). This function uses a Gaussian Kernel that is convolved with the spectrum. The filters are therefore applied to the ensemble of the data. This was done with the aim to remove long periodicities and to reduce the noise level. The light curve presents a large gap that could degrade the quality of the spectrum (window effect). The gap was removed before filtering the light curve by stitching the second segment to the first one separated by one cadence. Finally, the first time stamp was set to zero. The result is shown in panel (c) of Figure 3.

The last method started from the target pixel file to create a larger aperture. In general, light curves obtained from big apertures are more stable to small instrumental perturbations such as the loss of pointing of the satellite or the movement of the star during the observations. To build this larger aperture, contiguous pixels starting from the center of the target are selected. A new pixel is selected only if the integrated flux of the pixel has a negative gradient compared to the previous one (decreasing the flux from the center to avoid any polluting star) and with an average flux greater than a given threshold that has been established to 100 e-s^{-1}. Once this is done, an extra pixel at the top and an extra pixel at the bottom of the aperture are added to the 4 central rows, which contain several saturated pixels. By selecting these extra pixels, the resulting light curve has smaller dispersion around the mean between the days 1933.5 and 1936. The final aperture is shown in Figure 4. It is important to notice that no significant changes were found by adding more pixels to the central rows or by slightly changing the limit threshold of 100 e-s^{-1}.

To increase the duty cycle, instead of removing all points with a flag different to zero, we applied two different selections of the NASA quality flags. We kept all the points except those with a flags between 2 and 32 (Dark blue curve in panel (d) of Figure 3) or between 2 and 512 (magenta curve in panel (d) of the same figure). We then calibrated the two resulting light curves following García et al. (2011), removing outliers, correcting jumps and drifts. To convert the flux in parts per million and remove the low-frequency contribution, we used a triangular smooth with a window of half a day. Except for the big gaps in the middle of the run, all the rest were interpolated using inpainting techniques with a multiscale discrete cosine transform (García et al. 2014a; Pires et al. 2015). These two light curves are longer and with some more data in the middle of the run than the other three presented before.

The 20 s cadence data observed during sector 50 were also analyzed by the different methodologies described above. One of the results is shown in panels (e) and (e1) of Figure 3. In this case, the corrections are the same as the ones applied to produce the magenta curve shown in panel (d), but with a more stringent high-pass filter with a cut at 0.5 days.

In preparation of the seismic analysis, we computed the power spectral density (PSD). As shown in Figure 5, the PSD is dominated by flat noise above $\sim$200 μHz and a low-frequency slope below $\sim$60 μHz. Hence, the background can be characterized by two Harvey components (Harvey 1985) and a flat noise level. As expected, the high-frequency Harvey profile (related to convective noise) has an amplitude of around an order of magnitude smaller than the flat noise component. The low-frequency Harvey profile, with a knee at around 20 μHz, is probably related to magnetism and not convection.

GJ 504 is indeed a magnetically active star that was part of a large observational campaign, the HK Project, conducted at the MWO from 1966 to 1995 with the aim to search for stellar

[16] https://archive.stsci.edu/hlsp/tess-spoc

[17] https://archive.stsci.edu/missions/tess/doc/EXP-TESS-ARC-ICD-TM-0014.pdf

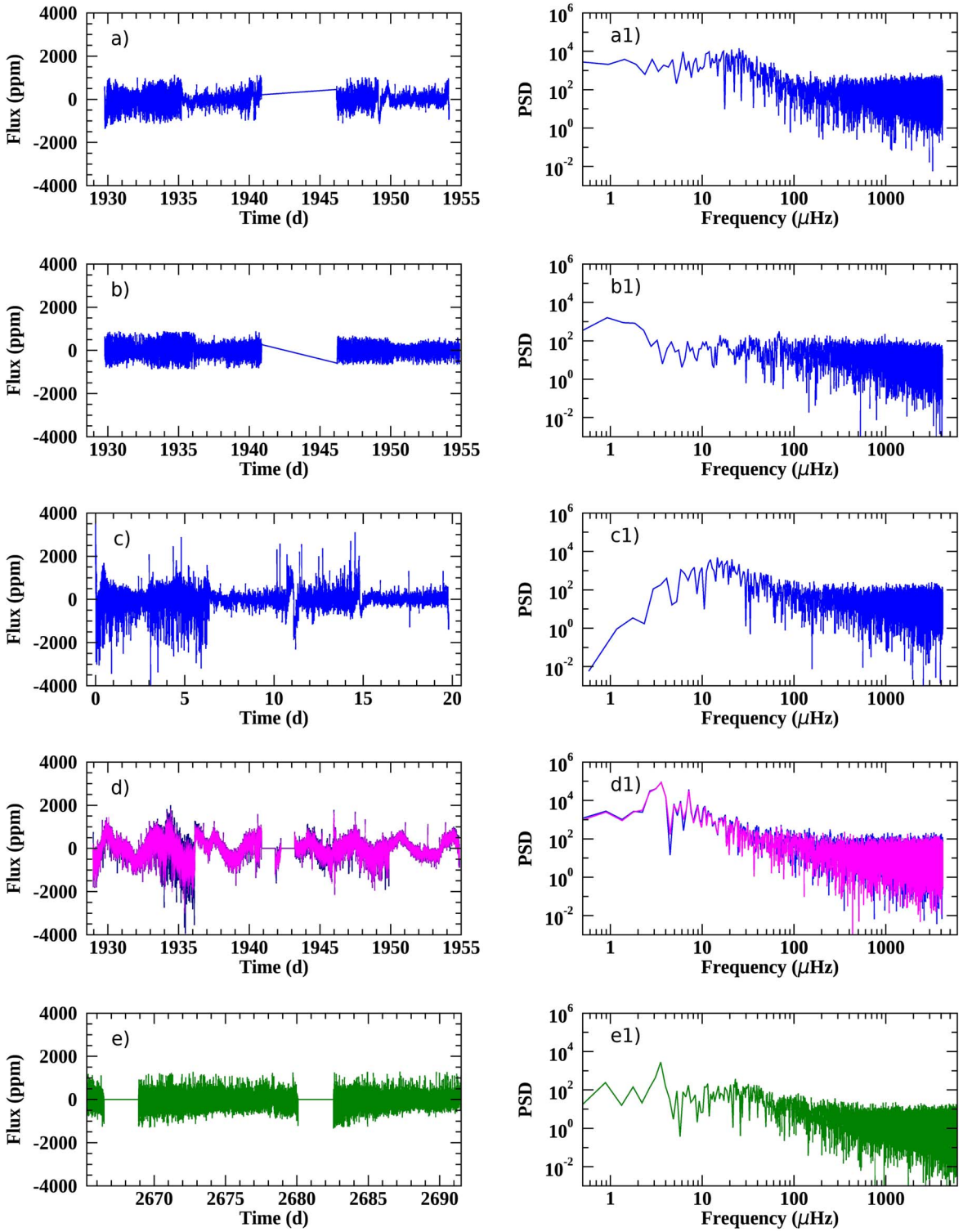

Figure 3. Seismically optimized light curves (left figures) and corresponding PSDs (right figures) from the analysis of the 120 s cadence data as explained in Section 3. The anomalous high scatter observed in this sector is related to the pointing jitter (Fausnaugh et al. 2020). Panels (e) and (e1) depict the results of the 20 s cadence data with the same method applied to get the magenta curves of panels (d) and (d1).

analogs to the solar cycle by studying stellar chromospheric activity and variability (Wilson 1968, 1978). These measurements, available from the National Solar Observatory website,[18] are expressed in term of the dimensionless S-index, defined as the ratio of emission in the Ca II H & K line cores to that in two nearby continuum reference bandpasses (for further details see, e.g., Vaughan et al. 1978; Egeland et al. 2017). For this star, within the MWO data set, about 1342 single measurements are provided in the time interval 1966–1995, allowing us to study its magnetic activity over a time period of nearly 30 yr.

[18] https://nso.edu/data/historical-data/mount-wilson-observatory-hk-project/

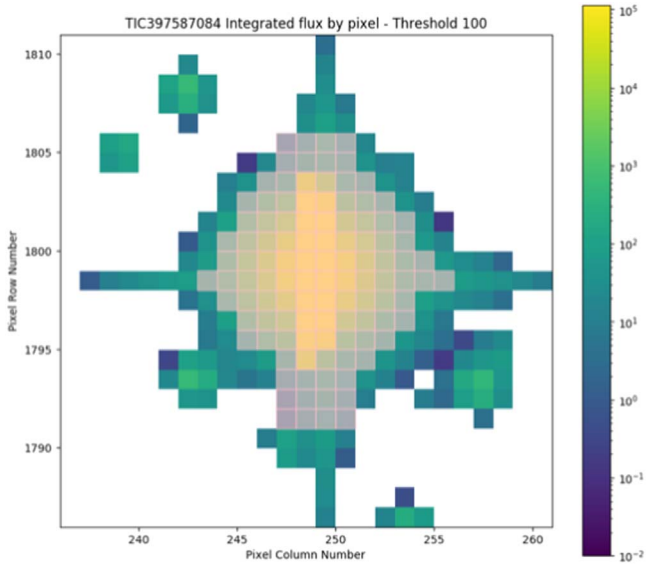

Figure 4. Enlarged mask used in the fourth calibration method described in Section 3. The selected pixels are depicted in gray.

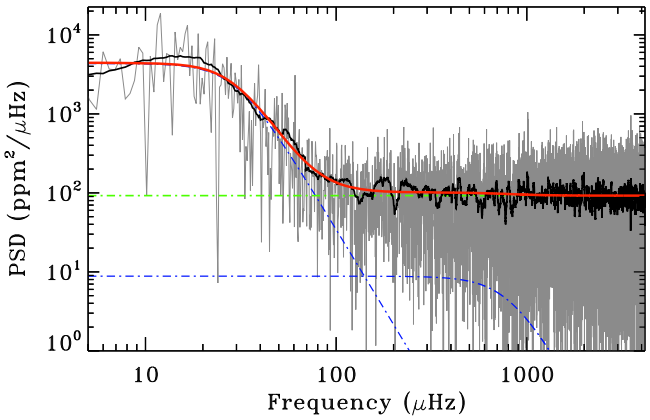

Figure 5. Power spectral density (light gray) with a smoothing overlaid (black curve) of the first seismically optimized light curve (shown in panel (a)) of Figure 3). The background fit is composed of two Harvey-like profiles (blue curves) and a flat noise level (green curve). The sum of the three components is indicated by the thick red line. No evidence of a Gaussian power excess is found.

4. Rotation and Magnetic Activity Analysis

4.1. Rotation

To determine the surface rotation period of GJ 504, a similar methodology as the one applied to the two last light curves described in the previous section is employed but this time smoothing the light curve using a triangular filter (double boxcar function). The width of each boxcar is a fifth of the total length. The obtained rotation period, $P_{\rm rot}$, is independent of the flags removed in the light curve because we are interested on the long periods, and thus the extra removed peaks with a bad flag do not affect the calculation. To look for $P_{\rm rot}$, a methodology combining three different techniques is used following, e.g., Santos et al. (2019, 2021). The first method performs a time-frequency analysis using a Morlet wavelet (Torrence & Compo 1998). The second utilizes an autocorrelation function (e.g., García et al. 2014b; McQuillan et al. 2014). The third method combines the first two to compute the composite spectrum (e.g., Ceillier et al. 2016). Hence, a modulation with a periodicity of (3.4 $\pm$ 0.25) days is found in the light curve (see Figure 6).

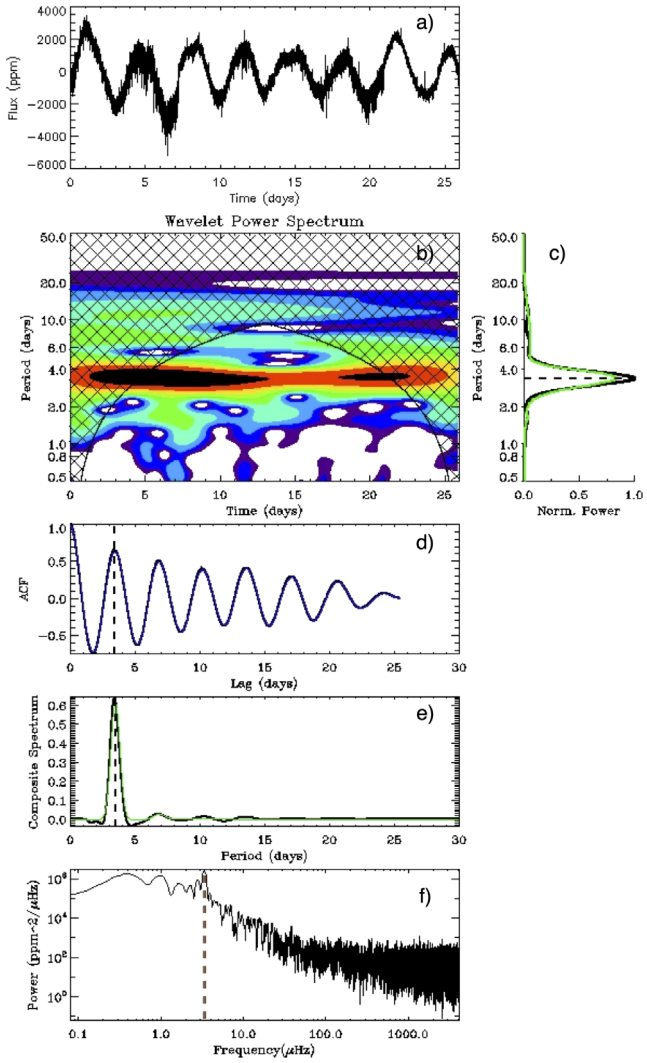

Figure 6. (a) TESS light curve for the rotation analysis. (b) Time-period analysis using wavelets. Black corresponds to high power and blue to low power. Black hatched area represents the region that cannot be sampled with the current length of the light curve. (c) Projection of the period-time analysis onto the period axis (black) and corresponding fits with multiple Gaussian functions (green). (d) Autocorrelation function. (e) Composite spectrum (black) and best Gaussian fit (green). (f) PSD in logarithmic scale. The black dotted line indicates the rotation-period estimate.

We also examined the Mount Wilson data to search for a potential rotational periodicity. The data consist of 1342 observations taken between 1966 March and 1995 June. Before searching for the presence of a periodicity in the S-index of GJ 504, we visually analyzed the available Mount Wilson data. We noted that 3 measurements taken in 1993, during the same night, are completely outside the mean range of variation (the average MWO S-index for this star is 0.313), with values that are approximately twice as large. We suspected that such scattered measurements could have arisen as result of an error in the data collection on that night; hence we chose to discard them in the following data analysis of the S-index. We then removed the three outliers with S-index values greater than 4σ above the mean, applied a simple linear detrending to the data to remove the lowest-frequency signal, and analyzed the resulting time series using both a discrete Fourier transform and

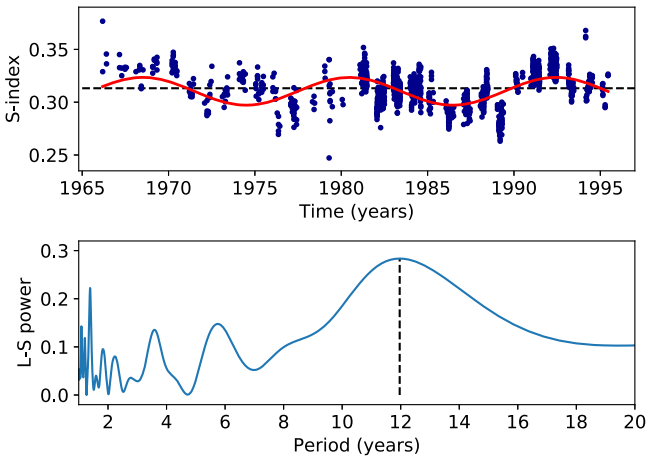

Figure 7. Top panel: Mount Wilson S-index measurements for the time interval 1966–1995. The dashed black line indicates the mean S-index. The red line shows the sinusoidal fit to the highest peak as provided by the periodogram in the bottom panel. Bottom panel: Lomb–Scargle periodogram of the S-index. The highest peak corresponds to a cycle period of $\simeq$12 *a*.

a Lomb–Scargle periodogram. Neither approach results in any significant signal in the range anticipated for rotation, and this conclusion is robust to the inclusion of the 3 deleted measurements. A longer high-quality time series would be necessary to reach any conclusion about the actual rotation period of this star. These results are confirmed with the light curve obtained during the observations of sector 50.

4.2. Magnetic Activity and Cycles

While determining the magnetic activity level and the eventually presence of a periodic variability of a star (i.e., a stellar cycle), a key role is played by long-term data sets providing measurements of chromospheric proxies. As known from literature, many stars other than the Sun show a chromospheric variability related to magnetic activity that exhibits periodic variations (see, e.g., Baliunas et al. 1995; Hall 2008). A periodic variability is typically visible also in the photospheric emission, whose phase difference with the chromospheric one reveals the activity dominant regime of the star, i.e., faculae-dominated (phase) or spot-dominated (antiphase; Radick et al. 1998; Reinhold et al. 2019). Before searching for the presence of a periodicity and to assess its level of magnetic activity, as in Section 4.1, we chose to discard the 3 outlier measurements in the following data analysis of the S-index.

In order to evaluate the magnetic activity level of the star, we first computed the average S-index over the whole time interval (1966–1995) as well as its extreme values. The data are shown in the top panel of Figure 7. The mean S-index is 0.313, while the minimum and maximum values are respectively 0.247 and 0.377. If we compare the mean value with the solar one for cycle 23 (0.170), as reported by Egeland et al. (2017), we can infer that the mean MWO S-index of GJ 504 is around 1.8 times that of the Sun. In addition, the variability in the S-index ($\sim$0.13), i.e., the difference between the maximum and minimum values, is greater than that of the Sun during a solar cycle ($\sim$0.02). We are, therefore, facing a star whose chromospheric activity level is much higher with respect to that of a reference star like the Sun, pointing toward a probable age smaller than the solar one due to the fact that chromospheric activity typically decreases as the star evolves (Skumanich 1972; Mamajek & Hillenbrand 2008; Fabbian et al. 2017; Gondoin 2018).

To search for a long-term periodic variation, the observations of the S-index from the MWO available for a large number of stars, constitute a very useful tool. To do that, we use an algorithm largely employed in astrophysics, the Lomb–Scargle periodogram (Lomb 1976; Scargle 1982), which, unlike the more classical fast Fourier transform analysis, allows to identify periodicity in unevenly sampled data, as in the case of the Mount Wilson observations. The computed Lomb–Scargle periodogram of GJ 504 is shown in the bottom panel of Figure 7. Despite the presence of some peaks at small timescales (1.39, 3.59, and 5.75 yr), partially due to the data sampling, the highest one corresponds to a main periodicity of 11.97 a. The corresponding false alarm probability is $7.97\ 10^{-93}$, indicating that the detected cycle period is statistically significant and unambiguous. This result indicates for this star the presence of a principal periodic chromospheric variability with a characteristic time quite similar to the Sun Schwabe 11 yr cycle, even if it is set to a higher level of activity compared to the latter.

In addition to measuring the magnetic activity of GJ 504 with spectroscopic data, we also computed the photometric magnetic activity index, $S_{\rm ph}$, using TESS data. Following Mathur et al. (2014a, 2014b), it is computed as the standard deviation of subseries of length $5 \times P_{\rm rot}$ to ensure that we are measuring the variability due to the magnetic activity. From that temporal $S_{\rm ph}(t)$, we take the mean value. Using the rotation period of 3.4 days found in Section 4.1, we obtain $S_{\rm ph} = (1231 \pm 7.8)$ ppm.

5. Searching for Solar-like Oscillations

Based on the spectroscopic parameters of GJ 504, we looked for the solar-like oscillations using the prediction from Sections 2.3 and 2.4. As seen in Figure 5, the modes are not obvious, and hence, we applied global seismic methods to look for the global seismic parameters.

In order to confirm the results obtained, the analysis of the power spectrum was independently performed by 4 teams who adopted different methods as described below.

The first method consisted of searching for the presence of oscillations in a region centered around 2000 μHz, as suggested by the former predictions for $\nu_{\rm max}$. For this purpose, we adopted the public tool DIAMONDS[19] (Corsaro & De Ridder 2014) coupled with the Background code extension[20] for estimating the level of the background signal. The background signal, as described in Corsaro et al. (2017), comprises two Harvey-like profiles accounting for a possible granulation-related signal and other variations at low frequency, a flat instrumental noise, and a Gaussian envelope of the solar-like oscillations. In particular we performed a Bayesian model comparison by means of the Bayesian evidence computed by DIAMONDS to select the best competing background model between one including the Gaussian envelope of the solar-like oscillations and one excluding it (see also Müllner et al. 2021). The resulting Bayes' factor suggests that the incorporation of an additional Gaussian profile is not statistically justified, meaning that in the light of the current data set we could not detect the presence of a power excess due to stellar oscillations in this star. This result is depicted in Figure 5, where no clear power excess due to stellar oscillations can be observed.

[19] https://github.com/EnricoCorsaro/DIAMONDS
[20] https://github.com/EnricoCorsaro/Background

With the second method (applied to the second set of light curves), we searched for local peaks in the amplitude spectrum, requiring a minimum separation between peaks of 20 μHz, and generated an upper envelope across those peaks using cubic spline interpolation. The location of the maximum of that envelope was taken to approximate $\nu_{\rm max}$, and was estimated by fitting a simple (linear + Gaussian) model and taking the center of the Gaussian to represent the location of the maximum. Uncertainties were estimated by repeating the procedure 1000 times with the minimum separation between peaks allowed to vary randomly between [0, 40] μHz. In each case, we also tried to estimate the large separation by performing an autocorrelation of the central 400 μHz of the amplitude spectrum. Unfortunately this process resulted in a peak envelope height not large enough to claim statistically significant detection.

The third pulsation search algorithm is an upgraded version of Benomar et al. (2012) and was applied to the third light curve described in Section 3. The first step consists in getting initial guesses for a Bayesian analysis that follows if pulsations are detected conclusively. A first power spectrum $F_{\rm noise}$ of the star is produced by heavily smoothing (boxcar smoothing of width $\approx$100 μHz) the original power spectrum. This allows to have an approximation of the noise background as pulsations (if any) are damped by the smoothing. A second spectrum $F_{\rm modes}$ is produced using a smoothing coefficient (boxcar smoothing of $\approx$0.8 μHz) optimized for revealing individual pulsations. The maximum of the amplitude of the ratio $F_{\rm modes}/F_{\rm noise}$ is then estimated by performing a local third-order polynomial fit. The FWHM of the polynomial curve is used to have a first estimate of the potential region for pulsations, and the height-to-noise ratio is used to evaluate the significance. We found only a marginal detection of pulsation. To confirm the detection, a fit of the power spectrum is performed. It involves describing the pulsations with a Gaussian envelope and the noise background with two Harvey-like profiles (Harvey 1985) and white noise. Unfortunately, the Bayesian maximum a posteriori estimates gave us a significance for pulsations below 1% when compared to a pure noise fit of the spectrum.

Another team analyzed two sets of light curves (LC1 and the one with our own aperture) with the A2Z pipeline (Mathur et al. 2010). Briefly, they looked for the mean large frequency spacing by computing the power spectrum of the power spectrum. We then fitted the background with three components: a Harvey law to model the granulation where the slope was fixed to 4, a Gaussian function for the modes, and the white noise. After subtracting the background without the Gaussian function, we fitted another Gaussian function to estimate the frequency of the maximum power. A blind run of the A2Z pipeline found some excess of power around 1000 μHz, but no frequency spacing that agrees with the global seismic scaling relations (Kjeldsen & Bedding 1995) was measured with a high level of confidence level. By forcing the pipeline to look around 2000 μHz, no Gaussian fit converged to obtain $\nu_{\rm max}$. These results lead to a nondetection of the modes with the A2Z pipeline.

Finally we also computed the envelope autocorrelation function (EACF) following Mosser & Appourchaux (2009). No detection of $\Delta\nu$ was done with this method. This is not surprising as the EACF and A2Z methods give similar results as shown for a sample of low signal-to-noise ratio targets where both methods were used (Mathur et al. 2022).

The analysis of the ultra short 20 s cadence data obtained during the TESS observations in sector 50 did not provide any clearer conclusion. We estimated the white noise level in the 20 s cadence data to be about 1.7 ppm^2μHz^{-1}, which is almost one order of magnitude (9.6 times) smaller than the one measured in the 120 s cadence data obtained from sector 23 (where we find 16 ppm^2μHz^{-1} instead). Despite this notable improvement in the level of noise, we were unable to obtain any statistically significant detection of a power excess due to solar-like oscillations. Moreover, we stitched together the data of both sectors to have a longer light curve. To do so, both light curves were filtered with a high-pass triangular filter with a cut at 0.5 days, and sector 50 data were rebinned to 120 s. To remove the long gap between the two sectors, the time of the first point of sector 50 was changed to 120 s after the last measure of sector 23. This has no influence on the p modes as they are expected to have shorter lifetimes than 2 yr. Once again, we were not able to detect any excess of power.

6. Discussion

6.1. Impact of Magnetic Activity on the Solar-like Oscillations

We discuss here the analysis of the TESS data and the nondetection of pulsation modes on the solar-like star GJ 504. While some of the analysis pointed toward a possible excess of power in the region around 2000 μHz, no reliable detection of solar-like oscillations can finally be reported. It is possible that this might be due to the high noise of the TESS data. However, another possible explanation can be attributed to the presence of a high level of magnetic activity. In fact, several authors have already shown that magnetic activity is responsible for suppression of solar-like oscillations as already found in several targets (e.g., García et al. 2010; Chaplin et al. 2011b; Mathur et al. 2019). The evolutionary stage, the estimate of the age, and the analysis of the magnetic activity indices of GJ 504 as developed in Sections. 4.2 reveal a level of magnetic activity typical of young solar-like objects (e.g., Böhm-Vitense 2007; Hall et al. 2007). In fact, the analysis of the chromospheric emission, through the S-index, has highlighted a fairly high level of magnetic activity (mean S-index = 0.313), $\sim$1.8 times that of the Sun. The study of the periodicities with the Lomb–Scargle algorithm has pointed out a main principal cycle at 11.97 a, in agreement with the 11.79 $\pm$ 0.28 a detected cycle by Boro Saikia et al. (2018), but also revealed the presence of other smaller amplitude cycles. The coexistence of different cycles is a typical characteristic of fast-rotating stars, where a higher number of dynamo modes are excited (Durney et al. 1981; Oláh et al. 2016), as it is the case of this star for which we found $P_{\rm rot} \simeq 3.4$ days.

Once the stellar rotation and the main activity cycle period are known, we can compute the ratio $P_{\rm cyc}/P_{\rm rot}$, a quantity that is known to be related to the dynamo number N_D (see, e.g., Soon et al. 1993; Baliunas et al. 1996). For stars older than 2.5 Gyrs, like the Sun, the quantity log ($P_{\rm cyc}/P_{\rm rot}$) is typically around 2 (see Figure 6 in Oláh et al. 2016), while we obtain 3.1. This result indicates that GJ 504 is an active star with an age smaller than the one where the transition from spot to faculae domination, associated with a Rossby number $R_0 \sim 1$ and an age $\sim$2.55 Gyr (Reinhold et al. 2019), is believed to happen. This is in agreement with our age estimation of 1.3 $\pm$ 1.3 Gyr. This is also consistent with the fact that Reinhold et al. (2019) found the photometric and

chromospheric variability to be out of phase ($\Delta\phi = 0.34$), indicating that the star is still in the spot-dominated activity regime, which characterizes the young and active stars.

Concerning our attempt to detect solar-like pulsations, we used the calibrated formula by Bonanno et al. (2014), to relate the Mount Wilson chromospheric S-index to the global oscillation amplitude $A_{\rm max}$. By using the mean S-index obtained in Section 4.2, we obtain for this star a regime of significant oscillation amplitude suppression (see, e.g., Figure 2 of Bonanno et al. 2014), defined by an expected global oscillation amplitude of $A_{\rm max} = 1.6$ ppm, which is rather low as compared to the level of background found in the data. This magnetic activity suppression likely justifies the nondetection of an oscillation power excess in the stellar power spectrum. Even in the case of minimum of activity, corresponding to an S-index of 0.247 (see Section 4.2), the expected oscillation amplitude would be 2.6 ppm, which is lower than the average background noise measured in the TESS data estimated to be 6.3 ppm from the background fitting we performed.

In addition, as obtained in Section 4.2, the $S_{\rm ph}$ of this star is (1231 ± 7.8) ppm during the TESS observations. Knowing that for the Sun, the average $S_{\rm ph}$ value is 166.1 ppm, we must conclude once more that GJ 504 appears to be very active (7.5 times higher than the Sun) in agreement with the result obtained from the spectroscopic observations. Comparing this level of activity with the stars with and without detection of modes (see Figure 10 of Mathur et al. 2019), only 3 stars with a detection of solar-like oscillations have an $S_{\rm ph}$ above 1000 ppm. For these stars, the comparison of the amplitude of the modes observed in the Kepler data and the predicted amplitude gives that $A_{\rm max,obs}/A_{\rm max,pred} \sim 0.8$ in average, varying between 0.70 and 0.93. This means that we can have a reduction from 7% to 30% in the amplitude of the modes. In the case that we are dominated by the noise, this can even add up to the explanation of the nondetection of the modes in this star. Note that these three Kepler stars are metal-poor (with [Fe/H] around -0.2dex), which according to Samadi (2011) can lead to higher amplitudes and could counterbalance the effect of the surface magnetic activity.

7. Conclusion

In this article, we present a new attempt to study the solar-like star GJ 504, observed by the space mission TESS and known to host an exoplanet with values of mass and radius not yet confirmed. Unfortunately, we did not succeed to characterize this star by means of asteroseismic techniques, since we did not find evidence for a clear excess of power.

With the aim to reach a substantial step forward in the characterization of this star by clearly detecting the solar-like oscillations, we proposed through the Director discretion time to observe it again during sector 50 with 20 s cadence mode. Based on TESS magnitude of 4.6552 ± 0.0073 (Stassun et al. 2019), the analysis of the 20 s cadence data should yield an improvement in photometric precision of $\simeq$30% due to the reduced influence of pointing jitter on cosmic-ray rejection for bright stars (Huber et al. 2022). Furthermore, the measured period $P_{\rm cyc} \simeq 12$ a of the main magnetic cycle of GJ 504 implies that the stellar magnetic cycle minimum should occur between 2022 and 2023, perhaps overlapping with TESS Sector 50, leading to the best conditions to minimize the amplitude-suppressing effect of magnetic activity. Unfortunately the analysis of the more recent data did not allow the hoped detection.

Table 4
The Parameters of GJ 504 as Derived by the Present Analysis Based on the Use of TESS and Mount Wilson Data

	Present Value
$P_{\rm cyc}$ (a)	11.97
$P_{\rm rot}$ (d)	3.4 ± 0.25
S-index	0.313 ± 0.07
$S_{\rm ph}$ (ppm)	1231 ± 7.8
Age (Gyr)	1.3 ± 1.3
$M/{\rm M}_{\odot}$	1.28 ± 0.07
$R/{\rm R}_{\odot}$	1.38 ± 0.20
$\Delta\nu$ (μHz)	98 ± 13

Note. $P_{\rm cyc}$ and $P_{\rm rot}$ are the magnetic activity cycle and the surface rotation period respectively. $M/{\rm M}_{\odot}$ is the mass of the star, $R/{\rm R}_{\odot}$ is the surface stellar radius, while $\Delta\nu$ is the theoretical large separation value as obtained by stellar modeling.

This nondetection can be explained by the high level of magnetic activity for the star. Indeed the spectroscopic analysis yields an S-index of 0.313, and the photometric analysis of the TESS light curves provides a magnetic proxy $S_{\rm ph}$ of 1231 ppm, both indices being much larger than the solar value of 0.170 and 161 ppm respectively. Given the values of the S-index and $S_{\rm ph}$, the modes are predicted to suffer an important decrease of their amplitudes, probably close to the noise level in the TESS observations.

Nevertheless, all the results that we have deduced by analyzing the photometric data by the TESS space mission, supported by the measurements collected by the Mount Wilson Observatory long-term campaign spanning nearly 30 yr and by the modeling procedures, have allowed us to get important conclusions on the large debated parameters of this target. In Table 4, we summarize the stellar parameters that best represent GJ 504.

First, the analysis of the three decades long Mount Wilson spectroscopic observations yields the detection of a main magnetic cycle of 11.97 a and, at least, two other smaller amplitude cycles of 5.75 and 3.59 a.

Further, the analysis of the Mount Wilson data did not allowed us to measure a stellar rotational period, while the TESS light curves show a clear modulation corresponding to $P_{\rm rot} = 3.4$ days.

The stellar radius and mass have been calculated from stellar models constrained on spectroscopic measurements of gravity, metallicity, and effective temperature only. Moreover, the value of the stellar radius results in agreement with independent measurements obtained in the present article by applying the SED and the SBCR methods, but also with the more accurate interferometric radius determined by Bonnefoy et al. (2018).

The age of GJ 504, as obtained by stellar modeling based on accurate spectroscopic fundamental parameters, appears to be $Age \leqslant 2.6$ Gyr in agreement, within the quoted uncertainties, with previous finding by D'Orazi et al. (2017) and Kuzuhara et al. (2013). In particular, the rotational period and the main magnetic cycle locate this G-type star in the regime of chromospheric activity dominated by the superposition of several magnetic cycles during which, as according to the not yet confirmed theory of van Saders et al. (2016) and Metcalfe & van Saders (2017), the magnetic braking should still be acting while the rotation is slowing down. This situation puts this target well before the magnetic transition, which would bring

this star at the age of about 4–5 Gyr to the shutdown of the magnetic braking reaching a low activity state.

Adopting this new age value, along with SPHERE JHK_1K_2 photometry for the companion (Bonnefoy et al. 2018) and the COND-AMES model atmospheres (Baraffe et al. 2003), we gather the companion mass and radius of $M_P = (16.5 \pm 4.8)$ M_{Jup} and $R_P = (1.00 \pm 0.03)R_{Jup}$ (the related errors are simply the standard deviation from the four photometric bands, so they are certainly underestimated). Hence, given the large uncertainty in age, we cannot confirm nor disprove from the present study whether GJ 504b is located in the brown dwarf or planetary regime. We confirm that the actual scenario is compatible with the hypothesis of engulfment of a substellar companion, as previously proposed by Fuhrmann & Chini (2015) and D'Orazi et al. (2017), necessary to explain the low rotational period and the age of the star. In fact, the orbits of the planets can change in time due to several mechanisms, such as tidal interactions, stellar winds, planet evaporation, leading a planet to be engulfed by its host star (Privitera et al. 2016; Benbakoura et al. 2019). As a planet moves to inner orbits, the conservation of angular momentum of the system imposes that a reduction in the orbital angular momentum is compensated by the increase in the stellar rotation. Benbakoura et al. (2019) showed that ultra hot Jupiters at closer orbital distances could spin up their hosts during the main sequence, while lighter planets (less than $1M_{jup}$) could not. A possible signature of a planet engulfment could be, for example, an anomalous metallicity. However, this target does not seems to be overmetallic, as shown in Table 1.

Finally, since we believe that GJ 504 might represent an ideal target also for the ESA/PLATO (Rauer et al. 2016) space mission, with scheduled launch in the end of 2026, we verified that it is included in the all-sky PLATO input catalog (Montalto et al. 2021), with the name of PIC DR1 35698898. However, according to the proposed PLATO fields presented in Nascimbeni et al. (2022), the portion of the sky where GJ 504 is located will not be considered for the first 2 yr of the PLATO observations.

This paper includes data collected with the TESS mission, obtained from the MAST data archive at the Space Telescope Science Institute (STScI). Funding for the TESS mission is provided by the NASA Explorer Program. STScI is operated by the Association of Universities for Research in Astronomy, Inc., under NASA contract NAS 526555. R.A.G. Acknowledges funding from the PLATO CNES grant. S.M. acknowledges support by the Spanish Ministry of Science and Innovation with the Ramon y Cajal fellowship number RYC-2015-17697 and the grant number PID2019-107187GB-I00. D.B. acknowledges support from the National Aeronautics and Space Administration under the Living With A Star program, grant number NNX16AB76G. R.R. is a PhD student of the PhD course in Astronomy, Astrophysics and Space Science, a joint research program between the University of Rome "Tor Vergata," the Sapienza University of Rome, and the National Institute of Astrophysics (INAF). The authors thank the anonymous reviewer for the valuable help in improving the manuscript.

ORCID iDs

Maria Pia Di Mauro https://orcid.org/0000-0001-7801-7484
Raffaele Reda https://orcid.org/0000-0001-8623-5318
Savita Mathur https://orcid.org/0000-0002-0129-0316
Rafael A. García https://orcid.org/0000-0002-8854-3776
Derek L. Buzasi https://orcid.org/0000-0002-1988-143X
Enrico Corsaro https://orcid.org/0000-0001-8835-2075
Othman Benomar https://orcid.org/0000-0001-9405-5552
Lucía González Cuesta https://orcid.org/0000-0002-1241-5508
Keivan G. Stassun https://orcid.org/0000-0002-3481-9052
Serena Benatti https://orcid.org/0000-0002-4638-3495
Valentina D'Orazi https://orcid.org/0000-0002-2662-3762
Luca Giovannelli https://orcid.org/0000-0001-7369-8516
Dino Mesa https://orcid.org/0000-0001-8467-1933
Nicolas Nardetto https://orcid.org/0000-0002-7399-0231

References

Addison, B. C., Wright, D. J., Nicholson, B. A., et al. 2021, MNRAS, 502, 3704
Angulo, C., Arnould, M., Rayet, M., et al. 1999, NuPhA, 656, 3
Baglin, A., Auvergne, M., Boisnard, L., et al. 2006, 36th COSPAR Scientific Assembly, Vol. 36 (Beijing: Beijing Institute of Technology (BIT)), 3749
Baliunas, S. L., Donahue, R. A., Soon, W. H., et al. 1995, ApJ, 438, 269
Baliunas, S. L., Nesme-Ribes, E., Sokoloff, D., & Soon, W. H. 1996, ApJ, 460, 848
Baraffe, I., Chabrier, G., Barman, T. S., Allard, F., & Hauschildt, P. H. 2003, A&A, 402, 701
Barnes, S. A. 2007, ApJ, 669, 1167
Battistini, C., & Bensby, T. 2015, A&A, 577, A9
Beck, P. G., Montalban, J., Kallinger, T., et al. 2012, Natur, 481, 55
Bedding, T. R. 2014, in Asteroseismology, ed. P. L. Pallé & C. Esteban (Cambridge: Cambridge Univ. Press), 60
Bedding, T. R., & Kjeldsen, H. 2003, PASA, 20, 203
Bedding, T. R., Mosser, B., Huber, D., et al. 2011, Natur, 471, 608
Belkacem, K., Goupil, M. J., Dupret, M. A., et al. 2011, A&A, 530, A142
Benbakoura, M., Gaulme, P., McKeever, J., et al. 2021, A&A, 648, A113
Benbakoura, M., Réville, V., Brun, A. S., Le Poncin-Lafitte, C., & Mathis, S. 2019, A&A, 621, A124
Benomar, O., Baudin, F., Chaplin, W., Elsworth, Y., & Appourchaux, T. 2012, MNRAS, 420, 2178
Böhm-Vitense, E. 1958, ZAp, 46, 108
Böhm-Vitense, E. 2007, ApJ, 657, 486
Bonanno, A., Corsaro, E., & Karoff, C. 2014, A&A, 571, A35
Bonnefoy, M., Perraut, K., Lagrange, A. M., et al. 2018, A&A, 618, A63
Boro Saikia, S., Marvin, C. J., Jeffers, S. V., et al. 2018, A&A, 616, A108
Borucki, W. J., Agol, E., Fressin, F., et al. 2013, Sci, 340, 587
Borucki, W. J., Koch, D., Basri, G., et al. 2010, Sci, 327, 977
Brown, T. M., Gilliland, R. L., Noyes, R. W., & Ramsey, L. W. 1991, ApJ, 368, 599
Buzasi, D., Carboneau, L., Hessler, C., Lezcano, A., & Preston, H. 2016, IAUFM, 29B, 673
Campante, T. L., Schofield, M., Kuszlewicz, J. S., et al. 2016, ApJ, 830, 138
Capitanio, L., Lallement, R., Vergely, J. L., Elyajouri, M., & Monreal-Ibero, A. 2017, A&A, 606, A65
Ceillier, T., van Saders, J., García, R. A., et al. 2016, MNRAS, 456, 119
Chaplin, W. J., Bedding, T. R., Bonanno, A., et al. 2011b, ApJL, 732, L5
Chaplin, W. J., Houdek, G., Appourchaux, T., et al. 2008, A&A, 485, 813
Chaplin, W. J., Kjeldsen, H., Bedding, T. R., et al. 2011a, ApJ, 732, 54
Chaplin, W. J., Sanchis-Ojeda, R., Campante, T. L., et al. 2013, ApJ, 766, 101
Chontos, A., Huber, D., Berger, T. A., et al. 2021, ApJ, 922, 229
Christensen-Dalsgaard, J. 1988, in IAU Symp. 123, Advances in Helio- and Asteroseismology, ed. J. Christensen-Dalsgaard & S. Frandsen (Dordrecht: Springer), 295
Christensen-Dalsgaard, J. 2008a, Ap&SS, 316, 13
Christensen-Dalsgaard, J. 2008b, Ap&SS, 316, 113
Corsaro, E., & De Ridder, J. 2014, A&A, 571, A71
Corsaro, E., Mathur, S., García, R. A., et al. 2017, A&A, 605, A3
Cutri, R. M., Skrutskie, M. F., van Dyk, S., et al. 2003, yCat, 2246, 0
da Silva, R., Porto de Mello, G. F., Milone, A. C., et al. 2012, A&A, 542, A84
Di Mauro, M. P. 2017, in Proc. of Frontier Research in Astrophysics—II PoS (FRAPWS2016), 269 (Trieste: SISSA), 29
Di Mauro, M. P., Christensen-Dalsgaard, J., Paternò, L., & D'Antona, F. 2004, SoPh, 220, 185
Donahue, R. A., Saar, S. H., & Baliunas, S. L. 1996, ApJ, 466, 384
D'Orazi, V., Desidera, S., Gratton, R. G., et al. 2017, A&A, 598, A19
Durney, B. R., Mihalas, D., & Robinson, R. D. 1981, PASP, 93, 537
Egeland, R., Soon, W., Baliunas, S., et al. 2017, ApJ, 835, 25

Fabbian, D., Simoniello, R., Collet, R., et al. 2017, AN, 338, 753
Fausnaugh, M., Burke, C. J., Caldwell, D. A., et al. 2020, TESS Data Release Notes: Sector 23, DR32, Tech. Rep. NASA/TM—2020—5001946, NASA, https://archive.stsci.edu/missions/tess/doc/tess_drn/tess_sector_23_drn32_v03.pdf
Fuhrmann, K. 2004, AN, 325, 3
Fuhrmann, K., & Chini, R. 2015, ApJ, 806, 163
Gaia Collaboration 2018, yCat, 1345, 0
Gaia Collaboration 2020, yCat, 1350, 0
Gandolfi, D., Barragán, O., Livingston, J. H., et al. 2018, A&A, 619, L10
García, R. A., & Ballot, J. 2019, LRSP, 16, 4
García, R. A., Ceillier, T., Salabert, D., et al. 2014b, A&A, 572, A34
García, R. A., Hekker, S., Stello, D., et al. 2011, MNRAS, 414, L6
García, R. A., Mathur, S., Pires, S., et al. 2014a, A&A, 568, A10
García, R. A., Mathur, S., Salabert, D., et al. 2010, Sci, 329, 1032
Gaulme, P., Jackiewicz, J., Spada, F., et al. 2020, A&A, 639, A63
Gondoin, P. 2018, A&A, 616, A154
Grevesse, N., & Noels, A. 1993, in Origin and Evolution of the Elements, ed. N. Prantzos, E. Vangioni-Flam, & M. Cassè (Cambridge: Cambridge Univ. Press), 15
Hall, J. C. 2008, LRSP, 5, 2
Hall, J. C., Lockwood, G. W., & Skiff, B. A. 2007, AJ, 133, 862
Harvey, J. 1985, ESASP, 235, 199
Huber, D., Bedding, T. R., Stello, D., et al. 2011, ApJ, 743, 143
Huber, D., Chaplin, W. J., Christensen-Dalsgaard, J., et al. 2013, ApJ, 767, 127
Huber, D., Chaplin, W. J., Chontos, A., et al. 2019, AJ, 157, 245
Huber, D., White, T. R., Metcalfe, T. S., et al. 2022, AJ, 163, 79
Iglesias, C. A., & Rogers, F. J. 1996, ApJ, 464, 943
Janson, M., Brandt, T. D., Kuzuhara, M., et al. 2013, ApJL, 778, L4
Jenkins, J. M., Twicken, J. D., McCauliff, S., et al. 2016, Proc. SPIE, 9913, 99133E
Jones, E., Oliphant, T., Peterson, P., et al. 2001, SciPy: Open source scientific tools for Python, http://www.scipy.org/
Kiefer, R., Schad, A., Davies, G., & Roth, M. 2017, A&A, 598, A77
Kjeldsen, H., & Bedding, T. R. 1995, A&A, 293, 87
Kjeldsen, H., Bedding, T. R., Arentoft, T., et al. 2008, ApJ, 682, 1370
Kuzuhara, M., Tamura, M., Kudo, T., et al. 2013, ApJ, 774, 11
Lallement, R., Vergely, J. L., Valette, B., et al. 2014, A&A, 561, A91
Lebreton, Y., & Goupil, M. J. 2014, A&A, 569, A21
Lebreton, Y., Goupil, M. J., & Montalbán, J. 2014, EAS, 65, 177
Li, T. D., Bi, S. L., Chen, Y. Q., et al. 2012, ApJ, 746, 143
Lomb, N. R. 1976, Ap&SS, 39, 447
Maldonado, J., Eiroa, C., Villaver, E., Montesinos, B., & Mora, A. 2015, A&A, 579, A20
Mamajek, E. E., & Hillenbrand, L. A. 2008, ApJ, 687, 1264
Mathur, S., García, R. A., Ballot, J., et al. 2014b, A&A, 562, A124
Mathur, S., García, R. A., Breton, S., et al. 2022, A&A, 657, A31
Mathur, S., García, R. A., Bugnet, L., et al. 2019, FrASS, 6, 46
Mathur, S., García, R. A., Régulo, C., et al. 2010, A&A, 511, A46
Mathur, S., Salabert, D., García, R. A., & Ceillier, T. 2014a, JSWSC, 4, A15
McQuillan, A., Mazeh, T., & Aigrain, S. 2014, ApJS, 211, 24
Mermilliod, J. C. 2006, yCat, 2168, 0
Messina, S., Pizzolato, N., Guinan, E. F., & Rodonò, M. 2003, A&A, 410, 671
Metcalfe, T. S., Monteiro, M. J. P. F. G., Thompson, M. J., et al. 2010, ApJ, 723, 1583
Metcalfe, T. S., & van Saders, J. 2017, SoPh, 292, 126
Metcalfe, T. S., van Saders, J. L., Basu, S., et al. 2020, ApJ, 900, 154
Metcalfe, T. S., van Saders, J. L., Basu, S., et al. 2021, ApJ, 921, 122
Mishenina, T. V., Pignatari, M., Korotin, S. A., et al. 2013, A&A, 552, A128
Montalto, M., Piotto, G., Marrese, P. M., et al. 2021, A&A, 653, A98
Mosser, B., & Appourchaux, T. 2009, A&A, 508, 877
Müllner, M., Zwintz, K., Corsaro, E., et al. 2021, A&A, 647, A168
Nascimbeni, V., Piotto, G., Börner, A., et al. 2022, A&A, 658, A31
Nielsen, M. B., Ball, W. H., Standing, M. R., et al. 2020, A&A, 641, A25
Nishiyama, S., Tamura, M., Hatano, H., et al. 2009, ApJ, 696, 1407
Oetjens, A., Carone, L., Bergemann, M., & Serenelli, A. 2020, A&A, 643, A34
Oláh, K., Kővári, Z., Petrovay, K., et al. 2016, A&A, 590, A133
Paunzen, E. 2015, yCat, 3580, A23
Pires, S., Mathur, S., García, R. A., et al. 2015, A&A, 574, A18
Pont, F., & Eyer, L. 2004, MNRAS, 351, 487
Privitera, G., Meynet, G., Eggenberger, P., et al. 2016, A&A, 593, L15
Radick, R. R., Lockwood, G. W., Skiff, B. A., & Baliunas, S. L. 1998, ApJS, 118, 239
Ramírez, I., Allende Prieto, C., & Lambert, D. L. 2013, ApJ, 764, 78
Rauer, H., Aerts, C., Cabrera, J. & PLATO Team 2016, AN, 337, 961
Reinhold, T., Bell, K. J., Kuszlewicz, J., Hekker, S., & Shapiro, A. I. 2019, A&A, 621, A21
Ricker, G. R., Winn, J. N., Vanderspek, R., et al. 2014, Proc. SPIE, 9143, 914320
Rogers, F. J., & Nayfonov, A. 2002, ApJ, 576, 1064
Salsi, A., Nardetto, N., Mourard, D., et al. 2021, A&A, 652, A26
Samadi, R. 2011, in The Pulsations of the Sun and the Stars, ed. J.-P. Rozelot & C. Neiner, Vol. 832 (Berlin: Springer), 305
Santos, A. R. G., Breton, S. N., Mathur, S., & García, R. A. 2021, ApJS, 255, 17
Santos, A. R. G., Campante, T. L., Chaplin, W. J., et al. 2018, ApJS, 237, 17
Santos, A. R. G., García, R. A., Mathur, S., et al. 2019, ApJS, 244, 21
Scargle, J. D. 1982, ApJ, 263, 835
Schofield, M., Chaplin, W. J., Huber, D., et al. 2019, ApJS, 241, 12
Silva Aguirre, V., Davies, G. R., Basu, S., et al. 2015, MNRAS, 452, 2127
Skemer, A. J., Morley, C. V., Zimmerman, N. T., et al. 2016, ApJ, 817, 166
Skumanich, A. 1972, ApJ, 171, 565
Soderblom, D. R., Hillenbrand, L. A., Jeffries, R. D., Mamajek, E. E., & Naylor, T. 2014, in Protostars and Planets VI, ed. H. Beuther et al. (Tucson, AZ: Univ. of Arizona Press), 219
Soon, W. H., Baliunas, S. L., & Zhang, Q. 1993, ApJL, 414, L33
Stassun, K. G., Collins, K. A., & Gaudi, B. S. 2017, AJ, 153, 136
Stassun, K. G., Corsaro, E., Pepper, J. A., & Gaudi, B. S. 2018, AJ, 155, 22
Stassun, K. G., & Torres, G. 2016, AJ, 152, 180
Stassun, K. G., & Torres, G. 2021, ApJL, 907, L33
Stassun, K. G., Oelkers, R. J., Paegert, M., et al. 2019, AJ, 158, 138
Stello, D., Bruntt, H., Preston, H., & Buzasi, D. 2008, ApJL, 674, L53
Stello, D., Cantiello, M., Fuller, J., et al. 2016, Natur, 529, 364
Tassoul, M. 1980, ApJS, 43, 469
Torrence, C., & Compo, G. P. 1998, BAMS, 79, 61
Torres, G., Andersen, J., & Giménez, A. 2010, A&ARv, 18, 67
Valenti, J. A., & Fischer, D. A. 2005, ApJS, 159, 141
Van Eylen, V., Lund, M. N., Silva Aguirre, V., et al. 2014, ApJ, 782, 14
van Saders, J. L., Ceillier, T., Metcalfe, T. S., et al. 2016, Natur, 529, 181
Vaughan, A. H., Preston, G. W., & Wilson, O. C. 1978, PASP, 90, 267
Wilson, O. C. 1968, ApJ, 153, 221
Wilson, O. C. 1978, ApJ, 226, 379
Wright, D. J., Chené, A.-N., De Cat, P., et al. 2011, ApJL, 728, L20